AFRL-RX-WP-JA-2017-0308

MODELING ENVIRONMENTAL DEGRADATION OF SIC/BN/SIC CMCS (PREPRINT)

Craig Przybyla and Michael K Cinibulk
AFRL/RX

Triplicane A. Parthasarathy
UES

Brain Cox and Olivier Sudre
Teledyne Scientific

6 February 2017
Interim Report

(STINFO COPY)

AIR FORCE RESEARCH LABORATORY
MATERIALS AND MANUFACTURING DIRECTORATE
WRIGHT-PATTERSON AIR FORCE BASE, OH 45433-7750
AIR FORCE MATERIEL COMMAND
UNITED STATES AIR FORCE

REPORT DOCUMENTATION PAGE

Form Approved
OMB No. 0704-0188

1. REPORT DATE *(DD-MM-YY)* 6 February 2017	2. REPORT TYPE Interim	3. DATES COVERED *(From - To)* 22 July 2013 – 6 January 2017

4. TITLE AND SUBTITLE
MODELING ENVIRONMENTAL DEGRADATION OF SIC/BN/SIC CMCS (PREPRINT)

5a. CONTRACT NUMBER
IN-HOUSE

5b. GRANT NUMBER

5c. PROGRAM ELEMENT NUMBER

6. AUTHOR(S)
1) Craig Przybyla and Michael K Cinibulk – AFRL/RX
2) Triplicane A. Parthasarathy – UES

5d. PROJECT NUMBER

5e. TASK NUMBER

5f. WORK UNIT NUMBER
X0S7

7. PERFORMING ORGANIZATION NAME(S) AND ADDRESS(ES)
1) AFRL/RX
Wright-Patterson AFB
Dayton, OH 45433

2) UES, Inc.
4401 Dayton Xenia Rd.
Beavercreek, OH 45432

8. PERFORMING ORGANIZATION REPORT NUMBER

9. SPONSORING/MONITORING AGENCY NAME(S) AND ADDRESS(ES)
Air Force Research Laboratory
Materials and Manufacturing Directorate
Wright-Patterson Air Force Base, OH 45433-7750
Air Force Materiel Command
United States Air Force

10. SPONSORING/MONITORING AGENCY ACRONYM(S)
AFRL/RXCC

11. SPONSORING/MONITORING AGENCY REPORT NUMBER(S)
AFRL-RX-WP-JA-2017-0308

12. DISTRIBUTION/AVAILABILITY STATEMENT
Distribution Statement A. Approved for public release: distribution unlimited.

13. SUPPLEMENTARY NOTES
PA Case Number: 88ABW-2017-0479; Clearance Date: 6 Feb 2017. This document contains color. The U.S. Government is joint author of the work and has the right to use, modify, reproduce, release, perform, display, or disclose the work.

14. ABSTRACT *(Maximum 200 words)*
Experimental data on the stress rupture behavior of SiC fiber based tows, minicomposites and ceramic matrix composites (CMCs) in air and moist air are interpreted using a mechanistic model. The kinetics of gaseous diffusion of oxygen and water from the environment through matrix cracks to internal fiber tows, the resulting oxidative loss of BN interphase, the oxidative strength degradation of the SiC fiber tows, and the oxidative sealing of matrix cracks are modeled and integrated within a numerical scheme to predict the stress-rupture behavior of the CMCs or minicomposites. The models for oxidation and/or volatilization of BN and SiC by oxygen and water use available relevant thermodynamic and kinetic data for reactions, vapor pressures, oxygen permeation, and boundary layer effects. Reported data on the kinetics of BN volatilization and SiC oxidation are captured to ensure model verification. The resulting model is compared with experimental data and is shown to capture available data on the stress-rupture data of SiC/BN/SiC CMCs in air and moisture containing atmospheres. An approach to link the model with higher order FEM-based models is suggested.

15. SUBJECT TERMS
SiC, fibers, BN coating, oxidation, air, moisture

16. SECURITY CLASSIFICATION OF:			17. LIMITATION OF ABSTRACT: SAR	18. NUMBER OF PAGES 30	19a. NAME OF RESPONSIBLE PERSON (Monitor) William Kennedy
a. REPORT Unclassified	**b. ABSTRACT** Unclassified	**c. THIS PAGE** Unclassified			**19b. TELEPHONE NUMBER** *(Include Area Code)* (937) 255-9987

Standard Form 298 (Rev. 8-98)
Prescribed by ANSI Std. Z39-18

REPORT DOCUMENTATION PAGE Cont'd

6. AUTHOR(S)

   3) Brain Cox and Olivier Sudre - Teledyne Scientific

7. PERFORMING ORGANIZATION NAME(S) AND ADDRESS(ES)

   3) Teledyne Scientific, 1049 Camino dos Rios
       Thousand Oaks, CA 91360

Modeling environmental degradation of SiC/BN/SiC CMCs

Triplicane A Parthasarathy[1,2], Brain Cox[3], Olivier Sudre[3], Craig Przybyla[1], Michael K Cinibulk[1],

[1]Air Force Research Laboratory, Materials and Manufacturing Directorate,

Wright-Patterson AFB, OH 45433-7817

[2] UES, Inc., Dayton OH 45432

[3]Teledyne Scientific, Thousand oaks, CA

Keywords: SiC, fibers, BN coating, oxidation, air, moisture

Abstract

Experimental data on the stress rupture behavior of SiC fiber based tows, minicomposites and ceramic matrix composites (CMCs) in air and moist air are interpreted using a mechanistic model. The kinetics of gaseous diffusion of oxygen and water from the environment through matrix cracks to internal fiber tows, the resulting oxidative loss of BN interphase, the oxidative strength degradation of the SiC fiber tows, and the oxidative sealing of matrix cracks are modeled and integrated within a numerical scheme to predict the stress-rupture behavior of the CMCs or mini-composites. The models for oxidation and/or volatilization of BN and SiC by oxygen and water use available relevant thermodynamic and kinetic data for reactions, vapor pressures, oxygen permeation, and boundary layer effects. Reported data on the kinetics of BN volatilization and SiC oxidation are captured to ensure model verification. The resulting model is compared with experimental data and is shown to capture available data on the stress-rupture data of SiC/BN/SiC CMCs in air and moisture containing atmospheres. An approach to link the model with higher order FEM-based models is suggested.

1.0   INTRODUCTION

SiC fiber based Ceramic Matrix Composites (CMC) are beginning to be used in aircraft gas-turbine engines and are being considered for use in land based turbine engines. The number of components in these engines that use CMCs is also expected to grow. The conditions in the gas turbine engine are oxidizing with significant moisture content (as high as 10%) at high pressures (tens of atmospheres) and temperatures reaching up to 1573K. It is also known that SiC and the interfacial coating BN can oxidize and volatilize under these conditions. Thus it is important to understand mechanisms that dominate the life of these CMCs in gas turbine engine environment, and to develop life prediction models that include environmental degradation.

At high temperatures (above roughly 1473K), the degradation is dominated by matrix erosion caused by reaction of the oxidation protective layer with moisture.[1] In the absence of matrix, SiC fibers are known to degrade rapidly. This has been experimentally studied by several investigators, and recently modeled to capture the available data. .[2-12] Thus matrix integrity is the key to protecting the fibers from environmental attack. CMCs are thus designed to be used at stresses below the matrix cracking stress. However matrix integrity cannot be assured due to imperfections in the matrix, stress overloads, foreign object damage, etc. At high temperatures the matrix cracks may be sealed by rapid oxidation of the matrix. But at intermediate temperatures, typically between 1073K and 1473K, before the matrix cracks can seal by oxidation, the degradation of fiber/matrix interface and the degradation of the fiber both through ingress of oxygen and moisture through the gaps in the matrix cracks, may dominate the life of CMCs.[13; 14] In this work we focus on modeling the degradation of the fiber, interface and matrix through matrix crack openings in SiC/BN/SiC CMCs.

Hi-Nicalon[TM] (HN) or Hi-Nicalon[TM] Type S (HNS) fibers dominate the commercial CMCs, and thus this work will be limited to CMCs using these fibers.[15] The degradation of these fibers has been studied extensively and recently modeled.[2-12; 16] The degradation kinetics of BN interface in the presence of moist air has also been experimentally studied and modeled.[17]

Similarly the diffusion of gases through matrix crack openings have been modeled for C/SiC composites.[18] This work exploits these data and prior models, refines the models as required, and combines them numerically to develop an integrated model that can capture all of the key degradation mechanisms of CMC degradation towards a life prediction model. The objective of this work is to obtain a quantitative environmental micromodel that can be used as a plugin with higher order thermos-mechanical models that are FEM based. The model should be able to predict CMC life as a function of stress at any combination of temperature, time, total pressure and partial pressures of oxygen and moisture, as well as fluid velocity.

The approach used here is to catalogue and model the known and anticipated mechanisms that dominate CMC degradation. The models developed for the various mechanistic processes are combined using a numerical algorithm that is iterative in nature to account for all the interdependencies of the processes that take place in parallel relative to each other. The oxidation model for the matrix and fiber borrows from prior modeling efforts on SiC oxidation[19-22]. The model includes loss of scale through evaporation of SiO, SiO_2 and $Si(OH)_4$ that form by reaction with moisture in the environment.[23] The model is fit to experimental data on SiC reported after exposure to dry oxygen, wet air, high pressure burner rig and steam over varying total pressures and fluid velocity.[19; 24] The model for oxidation of BN by oxygen and reactive volatilization in the presence of moisture were developed using thermodynamic data on $H_xB_yO_z(g)$, and gas phase diffusion kinetics, similar to the treatment by Jacobson et al.[17] The fiber oxidation kinetics and attendant strength loss were modeled as described in our recent work.[16] The effect of matrix crack was included by deriving the effective partial pressures of oxygen and moisture at the fiber tow, as a function of distance from the free surface and the crack opening. The matrix oxidation kinetics was used to determine the variation in crack opening with oxide scale formation. The assumptions and equations that constitute the model are presented first; this is followed by a section where the predictions are compared with the available experimental data. The final section discusses the

merits and limitations of the model including possible reasons for discrepancies and suggestions for future work.

2.0   THE MODEL

An overview of a model that seeks to predict the spatio-temporal evolution of damage in CMCs is shown in Figure 1. It is envisioned that a thermo-mechanical model can capture the effects of fiber architecture on the matrix crack evolution with time, temperature and stress. The thermo-mechanical model is not included in this work, as such models already exist or being developed with increasing fidelity and computational efficiency.[25; 26] The matrix crack opening, Δ_{COD}, the distance of fiber tows from the free surface, L_{surf}, and the traction force on the tow, F_{tow}, can be passed on from the thermo-mechanical model to an environmental micromodel. The environmental micromodel should be able to feed back to the thermo-mechanical model, the residual tow strength, F_c, the tow compliance $d\delta/dF$, and interfacial degraded length, L_{deg}, for a given external environmental condition of oxygen and moisture fractions, f_{O2}, f_{H2O}, total pressure, P_{tot}, and fluid velocity, V_{fluid}. The objective of the present modeling work is to develop a chemo-mechanical environmental micromodel that can in principle work in combination with a thermo-mechanical model to predict the life of a CMC.

2.1   Key mechanisms that dominate environmental degradation of CMCs

The degradation of CMCs is dominated by degradation of the fibers and the degradation of the interface coating, through reactions of the two with oxygen and moisture. The kinetics of these mechanisms are driven by oxidation and/or volatilization kinetics, which are dependent on the kinetics of gas phase diffusion of the reactants from the environment through an external barrier layer and then an internal pathway defined by matrix defects (Figure 1). The key mechanisms that dominate the degradation of CMCs are shown schematically in Figure 2.

There is no significant degradation of a dense matrix CMC in the intermediate temperature region, until a matrix crack forms and opens up allowing ingress of environmental gases. In a CMC with a BN interface, the oxidation of the B-containing phase is the most rapid. In the presence of

moisture the oxidation product B_2O_3, reacts with H_2O to form volatile gases with varying stoichiometry of $H_xB_yO_z$, depending on temperature and partial pressure of H_2O. This results in an interfacial gap (Figure 2a). This gap now allows oxygen and moisture to enter and oxidize the exposed SiC fiber, which in turn results in strength degradation (Figure 2b). This degradation causes the fiber tow to lose stiffness and strength (Figure 2c). Simultaneously, the gases passing through the matrix crack can and will react with the matrix crack faces themselves. The reaction product silica occupies more volume the SiC consumed in forming it, thus the crack opening decreases with time.(Figure 2d). Similarly the annular gap between the fiber and matrix decreases with time, as the fiber and matrix on either side of the gap oxidize and form their respective scales.(Figure 2e) Continued degradation of the interface depends on the width of this pathway until the pathway is completely closed, at which point the interface stops degradation. However, the fiber itself may continue to oxidize and degrade so long as the matrix crack opening is sufficiently wide and not closed by its own oxidation.

The development of an analytical model that incorporates all the interdependences of the various mechanisms is beyond the scope of this work. The approach taken here is to derive analytical expressions for each mechanism independently assuming a quasi-steady state condition, and then integrate the individual mechanistic models in time using a numerical algorithm. All the variables in the model are defined as shown tabulated in Table I.

2.1.1 Oxidation kinetics of fiber and matrix

The approach used for modeling of the oxidation of the fiber and matrix, in an environment of flowing gases containing oxygen and moisture, is the same as the one described for SiC-based fiber, detailed in our prior work.[16] Briefly, the oxidation kinetics was modeled using equations for oxygen flux across the scale, and for evaporative loss of scale from the surface. The effect of moisture on oxidation kinetics was modeled as due to enhanced oxygen permeability of the scale, and due to reactive volatilization of the scale as $Si(OH)_4$. The effect of external flow velocity is modeled by calculating a boundary layer thickness and matching the flux of oxygen across this layer

to the oxygen flux through the silica scale formed on SiC. The oxidation kinetics of SiC is modeled

using a permeation constant that is dependent on the partial pressure of H_2O. More details can be

found in the prior work[16] The results from that work, and used here, can be summarized as

follows.

$$\frac{dL_{scale}}{dt} = \frac{2}{3}V_{scale}J_{O_2(scale)} - V_{SiO_2}\left(J_{SiOH_4(v)} + J_{SiO_2(v)} + J_{SiO(v)}\right) \quad \dots (1)$$

$$J_{O_2-\text{scale}} = \Pi_{O_2-\text{scale}}\frac{P_{O_2(s)}}{L_{\text{scale}}} \quad \dots (2)$$

$$\Pi_{O_2-scale\ (H_2O)} = \Pi_{O_2-scale}\{1 + hP_{H_2O(s)}\} \quad \dots (3)$$

The reader is referred to the previous work for a complete derivation and equations for the various

parameters in the above equations.

In this work, as the fibers are embedded inside the matrix, there was no need to include the

effect of external flow on their oxidation kinetics. Similarly the effect of external flow did not affect

the oxidation kinetics of matrix on either side of the matrix crack. However, the flow did affect the

external matrix oxidation, and thus the $P_{O_2}^s$ at the surface of the matrix crack opening, which as

derived in our prior work [16], is given by the following equation.

$$P_{O2(s)} = \frac{D_{O_2}L_{\text{scale}}P_{O_2(a)}}{D_{O_2}L_{\text{scale}} + \delta_{bl}RT\Pi_{O_2-\text{scale}}} \quad \dots (4)$$

$$\delta_{bl} = 1.5L_{spec}N_{Sc}^{-1/3}N_{\text{Re}}^{-1/2} \qquad \text{where} \qquad N_{Sc} = \frac{\eta}{\rho D_{O_2}}; N_{\text{Re}} = \frac{\rho V L_{spec}}{\eta} \quad \dots (5)$$

The above equation shows how the oxygen partial pressure at the mouth of the matrix crack opening

is reduced by the boundary layer, δ_{bl}. It is seen that the effect is significant initially when the scale

formed on the matrix free surface l_{scale} is small, but the effect becomes small after the matrix forms a

reasonable scale.

The oxidation kinetics of the fiber and interface depend on the $P_{O_2,(t/m)}$, the partial pressure

of oxygen at the tow/matrix junction, which requires knowledge of $P_{O_2}(x)$, where x is the distance

from the free surface. The modeling of gaseous diffusion through matrix crack which gives $P_{O_2}(x)$ is addressed next.

2.1.2 Gaseous diffusion through matrix crack

Consider, as shown in Figure 3, a small element along the matrix crack at any arbitrary time under quasi steady-state conditions. The inward flux of oxygen diffusing down the matrix crack into this element, less the oxygen flux diffusing out of this element should equal the oxygen flux through the matrix oxide scale of thickness $L_{scale,cod}$ on either side. This is given by the following equation.

$$10^5 \frac{D_{O_2}}{RT} \Delta_{COD}(t) \frac{d^2 P_{O_2}}{dx^2} = 2 P_{O_2} \frac{P_{O_2} - P_{O_2/SiO_2}}{L_{scale,cod}} \quad \text{or} \quad \frac{d^2 P_{O_2}}{dx^2} = \frac{2 P_{O_2} RT}{10^5 L_{scale,cod} \Delta_{COD} D_{O_2}} P_{O_2} \quad \dots (6)$$

Neglecting the equilibrium partial pressure of oxygen at SiC/SiO$_2$ interface, P_{O_2/SiO_2} ,the solution for the equation is:

$$P_{O_2}(x) = C1 \exp\left(-x \sqrt{\frac{2 P_{O_2} RT}{10^5 L_{scale,COD} \Delta_{COD}(t) D_{O_2}}}\right) + C2 \exp\left(x \sqrt{\frac{2 P_{O_2} RT}{10^5 L_{scale,COD} \Delta_{COD}(t) D_{O_2}}}\right) \dots (7)$$

Applying the boundary conditions that the P_{O_2} at the surface is $P_{O_2}^s$, and that at infinite distance is zero, the solution reduces to the following.

$$P_{O_2}(x) = P_{O_2}^s \exp\left(-x \sqrt{\frac{2 P_{O_2} RT}{10^5 L_{scale,cod} \Delta_{COD} D_{O_2}}}\right) \qquad \dots (8)$$

This equation gives the oxygen partial pressure as a function of distance from the free surface along the matrix crack of a given Δ_{COD} at time t. Note that the opening for gaseous diffusion, Δ_{COD}, itself changes as $L_{scale,cod}$ increases with time.
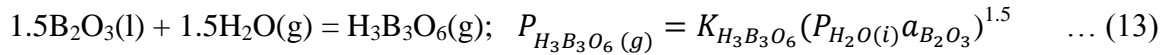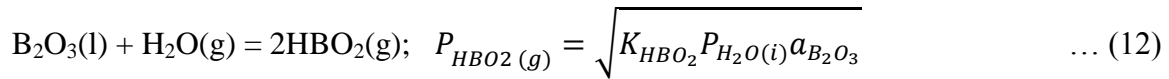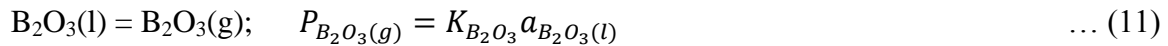
$$\Delta_{COD}(t) = \Delta_{COD}(0) - 2 L_{scale,cod}(t) \qquad \dots (9)$$

As mentioned earlier, the effects of time dependence of $L_{scale,cod}$ are taken into account through numerical integration.

2.1.3 BN interface degradation

The BN interface is known to degrade by oxidation and by reactive volatilization in the presence of moisture, as given by the following reactions.[17]

$$2BN + 3/2 O_2 = B_2O_3(l) + N_2(g) \qquad \dots (10)$$

$$B_2O_3(l) = B_2O_3(g); \qquad P_{B_2O_{3(g)}} = K_{B_2O_3}a_{B_2O_{3(l)}} \qquad \dots (11)$$

$$B_2O_3(l) + H_2O(g) = 2HBO_2(g); \quad P_{HBO2\,(g)} = \sqrt{K_{HBO_2}P_{H_2O(i)}a_{B_2O_3}} \qquad \dots (12)$$

$$1.5B_2O_3(l) + 1.5H_2O(g) = H_3B_3O_6(g); \quad P_{H_3B_3O_6\,(g)} = K_{H_3B_3O_6}(P_{H_2O(i)}a_{B_2O_3})^{1.5} \qquad \dots (13)$$

The rate constants for the reactions were obtained from Barin's compendium. [27] The vapor

pressures of the three gases vary with temperature, with HBO_2 dominating at temperatures above

800°C, and $H_3B_3O_6$ dominating at lower temperatures; thus only one of the species needed to be

modeled for a given temperature and partial pressure of moisture. From prior work, the BN loss

kinetics is known to be dominated by diffusive flux of the gaseous reaction products. [17]

Modeling the kinetics was based on balancing the flux of gases, as shown in Figure 4. The flux of

gaseous reaction products is proportional to their partial pressures.

$$J_i = 10^5 \frac{D_i}{RT}\frac{P_i}{L_{deg}} \qquad \dots (14)$$

The flux of oxygen and H_2O are proportional to their partial pressures at the two/matrix interface.

$$J_{O_2(g)} = 10^5 \frac{D_{O_2}}{RT}\frac{P_{O_2,(t/m)} - P_{O_2,i}}{L_{deg}} \qquad \dots (15)$$

$$J_{H_2O(g)} = 10^5 \frac{D_{H_2O}}{RT}\frac{P_{H_2O,(t/m)} - P_{H_2O,i}}{L_{deg}} \qquad \dots (16)$$

As per reactions 11 through 13, the flux of gases must obey the following for quasi-steady state

equilibrium.

$$J_{O_2} = \frac{3}{2}J_{B_2O_3} + \frac{3}{4}J_{HBO_2} + \frac{9}{4}J_{H_3B_3O_6} \qquad \dots (17)$$

$$J_{H_2O} = \frac{1}{2}J_{HBO_2} + \frac{3}{2}J_{H_3B_3O_6}$$

Equation 17 yields

$$P_{O_2,i} = \frac{-6D_{B_2O_3}P_{B_2O_3} - 9D_{H_3B_3O_6}P_{H_3B_3O_6} - 3D_{HBO_2}P_{HBO_2} + 4D_{O_2}P_{O_2,(t/m)}}{4D_{O_2}} \qquad \dots (18)$$

The solution for $P_{H_2O,i}$ is much more complex, and thus not shown here, when multiple species of

$H_xB_yO_z$ were included. It was determined that a numerical solution will the best approach.

Fortunately, it was found that the vapor pressure of HBO_2 dominated at temperatures above

~750°C, and thus assuming only this specie as rate controlling, the following expression could be derived.

$$P_{H2O,i} = \frac{1}{8D_{H2O}^2}\left(a_{B2O3}D_{HBO2}^2 K_{HBO2} + 8D_{H2O}^2 P_{H2O,(t/m)}\right.$$

$$\left. + \sqrt{a_{B2O3}}D_{HBO2}\sqrt{K_{HBO2}}\sqrt{a_{B2O3}D_{HBO2}^2 K_{HBO2} + 16D_{H2O}^2 P_{H2O,(t/m)}}\right)$$

$$\dots \text{ (18)}$$

From equation 8,

$$P_{O_2,t/m} = P_{O_2}^s \exp\left(-L_{surf}\sqrt{\frac{2P_{O_2}\text{RT}}{10^5 L_{scale,cod}\Delta_{COD}D_{O_2}}}\right) \qquad \dots \text{ (19)}$$

$P_{H_2O,(t/m)}$ was taken to be the same as $P_{H_2O,a}$ for two reasons. First, H_2O is not consumed by matrix oxidation of crack faces, and second, the flux in of H_2O is not rate limiting, as the vapor pressures of the gaseous products are orders of magnitude lower than that of H_2O, and thus have much lower flux. The slowest of the fluxes will be rate limiting. Thus the rate of change of the interface length that is degraded is given by

$$d(L_{deg})/dt = (1\text{-}t_{gap}/t_{BN})V_{BN} J_{\text{i-rate lim}} \qquad \dots \text{ (20)}$$

In the equation 16, the factor $(1\text{-}t_{gap}/t_{BN})$ accounts for the fact that the rate of B_2O_3 formed and the corresponding oxygen flux required is determined by t_{BN}/t_{gap} , where t_{gap} is the reduced interfacial gap, resulting from the scales formed on fiber and matrix. The parameter t_{gap} varies with time, as given by the following.

$$t_{gap} = t_{BN} - L_{scale,f} - L_{scale,m} + R_f + R_m \qquad \dots \text{ (21)}$$

The scale thicknesses, $L_{scale,f}, L_{scale,m}$ are obtained as described by equation 1 and the attendant recessions $R_{scale,f}, R_{scale,matrix}$ are calculated using the molar volumes of SiC and SiO_2 as detailed in our prior work.[16] In addition the effect of the reduced gap on gaseous diffusion, including Knudsen effect needs to be included, and was modeled as follows.

$$D_{eff} = (D_k^{-1} + D_{1-2}^{-1})^{-1} \qquad D_k = \frac{4}{3}\left(\frac{8RT}{\pi M}\right)^{1/2}\frac{t_{gap}}{2} \qquad \dots \text{ (22)}$$

The gas phase diffusivity was obtained using Chapman-Enskog equations and the multigas diffusivity was obtained using the following rule of mixtures for diffusion.

$$D_{1,(2,..i)} = \frac{1}{\sum\limits_{i}^{i \neq 1}(x_i / D_{1-i})} \quad ; \quad x_i = \frac{n_i}{\sum\limits_{j}^{j \neq 1} n_j} \qquad \qquad \dots \ (23)$$

2.1.4   Fiber tow degradation

The model for fiber oxidation kinetics, recession and scale thicknesses and attendant strength loss was borrowed from prior work.[16] The values of $P_{O_2,(t/m)} \ and \ P_{H_2O,(t/m)}$ were used to calculated the fiber strength degradation. To extend the fiber strength degradation to that of a fiber tow, a numerical approach was used to handle the statistical aspects of the failure of a tow when subjected to environment and a load. The Weibull statistics of fiber bundles is used along with the time dependent loss in strength of fibers from grain growth and oxidation to derive the residual tow strength as a function of time and temperature. Thus a loaded tow will fail by a sequential failure of one fiber at a time, shedding load globally to other fibers. The sequence will depend on the Weibull distribution of strengths, and the time dependent loss in strength of the same. The resulting numerical model can predict the time dependent extension in the tow caused by sequential failure, which appears like a creep curve but is due to fiber failures. The model predicts a residual strength and fiber tow stiffness at any time during the thermo-environmental exposure, to be used in higher order thermos-mechanical model as envisioned. In addition, the model can be used to capture/verify stress-rupture data on fiber tows and mini-composites that have been pre-cracked to expose internal fibers.

In experimental work, sometimes the fiber tows have been found to bond to each other due to oxidation. In such situations, a more brittle or flat fracture has been observed implying that the fibers do not obey a global load sharing model. Instead fibers that are bonded fail together when the weakest fiber in the bundle fails. The extent of such bonding varies from specimen to specimen, and in CMCs this may vary from location to location and may be unpredictable, resulting in scatter in the data. To account for this, two extreme statistics were used to predict the bounds of stress-rupture

lives, one using a local load sharing model (LLS) and the other a global load sharing (GLS) model. In predicting the lower bound (LLS) the weakest fiber was taken to determine the residual strength of rupture time. The Weibull statistics with global load sharing (GLS) was used to predict the upper bound.

3.0   MODEL PREDICTIONS AND VALIDAITON

3.1   Parameters

A list of variables used in the model is shown in Table I with a brief description and the values that were used in the model predictions. The model parameters used for fiber oxidation and attendant strength degradation were the same as detailed in our prior work.[16] All required thermodynamic quantities are available in the compendium by Barin.[27] The thermodynamics of Si-O-H system was taken from the works of Jacobson et al. and Plyasunov [28; 29] The diffusivities of gases in a multigas solution were calculated using parameters given by Svehla, and the methods outlined in our prior work.[30; 31] To capture the data on fibers which do not form pure silica scales, and which have been shown to oxidize faster than pure SiC, the oxygen permeability was adjusted. The temperature dependent oxygen permeability used for both HN and HNS was 8×10^{-12} exp(-167000/RT) moles/m-s-Pa. The permeability used for pure silica was 10^{-12} exp(-172998/RT) moles/m-s-Pa; the parameter h that accounts for the dependence on P_{H_2O} (Eqn.10) was 25 based on the best fit to experimental data. The temperature dependence for HN and HNS for permeability is consistent with the range reported for molecular oxygen diffusion within the scale formed on HN as compiled by Shimoo et al.[32] The matrix oxidation rate was taken to be the same as that of the fiber in simulating behavior of CVI matrix CMCs, and it was taken to be twice as high in simulating PIP based CMCs where B-rich phases are often present in the matrix.

3.2   Comparison of Model Predictions with Experimental Data

A numerical code was written in Fortran that integrates all of the above mechanism-based semi-empirical models in proper sequence using small increments in time interval to capture the combined effects of time-temperature-environment history the length of degraded zone along the

interface, the residual tow strength, the stiffness of the tow, and rupture life. The model requires as input the matrix crack opening, the distance of the fiber tow from the free surface, and the force on the tow. As mentioned earlier, these inputs are expected from a thermos-mechanical model for a prediction of the spatio-temporal evolution of damage in CMCs. However, the spatially averaged behavior of a CMC can be predicted using experimental values for crack opening, sample thicknesses and applied stress. Thus in this work, the spatially averaged model predictions are compared with available experimental data to examine the model validity. A key limitation in doing so is the absence of experimental data on the matrix crack opening; thus model predictions were made for different assumed values to capture possible trends.

3.2.1 Length of interface degraded zone, L_{deg}

Jacobson et al. conducted experiments on sectioned composites exposed to controlled moisture containing environment to study the depth of BN oxidation/volatilization with time at temperature.[17] Their results are shown compared with model predictions in Figure 5. The matrix crack opening was taken to be sufficiently large so no sealing occurs; note that interfacial gap can and does seal by oxidation of fiber and matrix on either side of the interface. The length of degradation was measured at two different temperatures, two different BN thicknesses and two different ratios of H_2O/O_2 in the environment. Figure 5a shows the model compared with experimental data for 10% H_2O/O_2 ratio at 700°C and Figure 5b shows the comparison for 1% H_2O/O_2 ratio at 700°C and 800°C. The BN interphase thickness was of the order of 0.5 micron for the results shown in Figure5a, and 1.0 micron for the results in Figure 5b. The model is seen to predict reasonably well all of the data and capture the correct dependence of the degradation length on temperature, moisture content and BN coating thickness.

3.2.2 Stress rupture behavior of HN tows and minicomposites

There have been three works in the literature that have reported on the stress rupture behavior of HN tows and minicomposites with BN as interphase.[33-35] The model was exercised to predict the behavior of fibers directly exposed to environment, which was then used to calculate

fiber tow behavior by assuming either GLS or LLS in order to capture the bounds. The minicomposites tested were pre-cracked to expose fibers to environment. Thus the model predictions were made assuming that the COD was large. The results are shown in Figure 6. The stress shown is normalized with respect to the room temperature as-received strength. It is seen that the model captures the bounds of the data obtained at 973K, 1173K, 1223K and 1473K. In general, the data on tows appear to be close to the model predictions for GLS, while the data on minicomposites fall close to the model predictions for LLS. In the work on minicomposites, the authors make specific reference to the observation of fiber failure with limited or no pullout, implying LLS being appropriate to describe their failure.

3.2.3 Stress rupture behavior of HN/BN/SiC CMCs

There have been two sets of unpublished data on the stress-rupture behavior of a commercial CMC, S200H, which uses BN coated HN and a PIP processed SiC matrix.[36; 37] The stress rupture data were obtained at 1173K, 1198K, 1473K and 1573K in ambient air containing ~80%RH, which is about 3 mol% H_2O and thus used in the model. The model predictions along with the data are shown in Figure 7. The model assumed that the matrix oxidation kinetics was the same as that of the fiber, and that the fiber tows were 2 mm from the free surface. The predictions were made for two different initial crack openings, $\Delta_{COD}(0)$ of 1μm and10μm. The model is able to capture the data within the two bounds given by GLS and LLS for the data measured 1473K by Zawada et al.[37]. The data is close to LLS for the data measured at 1198K and 1573K, by Marshall et al.[36] Among the data from shown in Figure 7(b), it is seen that there is significant scatter in life. In particular, two identical samples were tested at 1473K under a stress of 256 MPa. One of them failed in 2.53h, while the other was considered a run-out after 20h. The latter was then tested at room temperature for residual strength. The fracture surfaces of the two CMC samples are shown in Figure 8. It can be seen that the fiber fracture is largely correlated resulting in a flat fracture for the sample with a short life, while long pullouts are observed in the run-out sample. Thus they

support the model which predicts the sample with short life to be dominated by LLS, and the one with a run-out to be dominated by GLS.

Figure 9 shows the model predictions for residual strength of S200H CMCs after exposure to ambient air under stress. The data of Marshall et al. are shown compared with the model predictions for temperatures and stresses of 1573K/80 MPa, 1573K/120 MPa, 1473K/240 MPa and 1173K/80 MPa. The GLS and LLS bounds predicted by the model are able to capture the data reasonably well. The data for 1173K, 80 MPa and 1573K, 120 MPa seem to be closer to LLS prediction, while the other two fall closer to GLS. The reasons for this are not clear.

4.0   DISCUSSION

The need for lifing models for ceramic matrix composites (CMCs), which are increasingly finding applications in the turbine engine components, is clear. The turbine engine condition is characterized by an oxidizing atmosphere with significant amounts of water, at high total pressures. The life under such conditions is dominated by environmental damage that is cumulative with respect to time at temperature. While different regimes of degradation exist, this work concentrated on the stress-rupture behavior of CMCs in the temperature range of 1173K-1573K, where both fibers and interfaces are known to degrade at stresses above matrix cracking stress.

A chemo-mechanical micromodel for the environmental degradation of SiC/BN/SiC CMCs in dry and moist air at ambient and turbine engine conditions has been developed by identifying key mechanisms of degradation, modeling the individual mechanistic processes and integrating the models numerically. The degradation of fiber strength and interface have been shown to capture available literature data. Further, the integrated model is shown to capture available stress-rupture data and residual strength data on a commercial CMC, based on spatially averaged predictions. When further integrated with a thermo-mechanical discrete damage model, the present model is expected to predict the spatio-temporal evolution of damage in CMCs. It remains to use the model to examine the effects of individual variables to glean the important parameters that might influence the life of CMCs under turbine engine conditions.

4.1 Parameteric Studies

4.1.1 Effect of distance of fiber tow from the free surface

Figure 10 shows the model predictions for stress rupture at 1473K for two different initial crack opening displacements, (a) $\Delta_{COD}(0)=10\mu m$ and (b) $\Delta_{COD}(0)=1\mu m$. In each of these plots, the model predictions for different values of L_{surf} are shown along with experimental data on S200H measured by Zawada et al.[37] It is seen that for very large crack opening, as might be appropriate for a porous matrix, the distance from the free surface has no significant in the range of 0.1mm to 10mm. However when the crack opening is smaller, at 1 micron, which is at the high end of dense matrix composites, there is a significant effect of the distance of the tow from the free surface.

4.1.2 Effect of temperature and environment on interface degradation length

To study the effect of environment on interface degradation length, the model was exercised suppressing the matrix crack sealing effect by keeping the opening large. Figure 10c shows the effect of temperature and on the length of degraded interface length for a CMC with 0.3 micron BN coating, exposed to humid ambient air. It is seen that the interface degradation reaches a limiting value for higher temperatures but at 973K, the degraded length continually increases even up to 1000h. The limiting value at higher temperatures arises from the sealing of the interfacial gap by the oxidation of fiber and matrix on either side of the BN denuded interfacial region. Beyond 1173K, there is no significant effect of temperature. In Figure 10d, the degradation kinetics in a typical turbine engine environment is shown. At 10% moisture and 10atm total pressure, the degradation length rises rapidly but the simultaneous rapid oxidation of fiber and matrix results in sealing at very early times. The limiting values for degradation lengths are smaller in turbine engine conditions, although the time taken to reach the same is much shorter.

4.1.3 Effect of temperature on stress-rupture

Figure 11 shows the model predictions for the stress-rupture behavior of SiC/BN/SiC CMCs in an environment that represents turbine engine conditions. The degradation is faster at 1473K, but

the time taken for matrix crack sealing is shorter. At 1073K, the degradation is slower, but significant degradation can occur before the matrix crack is sealed.

4.2   Model Strength and Weaknesses

The strength of the model is in identifying from literature search the key mechanisms, building models for known individual mechanistic processes of environmental degradation of CMCs, and integrating them within a numerical framework to predict the stress-rupture lives of SiC/BN/SiC CMCs. Further the model derives credence from its ability to capture experimental data on fiber degradation, interface degradation kinetics, and available data on stress-rupture of mini-composites and CMCs. The model is able to extend data obtained under ambient conditions to turbine engine conditions, using thermodynamic and kinetic models that contain dependencies on partial pressures of oxygen and moisture, as well as total pressure and fluid velocities. Finally the model allows for the possibility of importing it to a thermos-mechanical damage model in order to be able to capture the spatio-temporal evolution of environmental damage in CMCs, based on the microstructure of the CMC.

There are some limitations of the model that need to be pointed out. The model assumes an idealized geometry for matrix crack and fiber tow bridging the crack. The tortuosity of the matrix crack is ignored. The model also does not provide for possible permeation of environment through defects in the matrix such as pores, which are often present in commercially processed CMCs that utilize polymer infiltration for building the matrix. The model cannot be fully validated at this time due to the lack of information on crack opening displacements, which have thus far not been measured reliably. A constant value is assumed for crack opening and distance of tows from surface; clearly an approximation. A pathway to linking the model with a finite damage thermos-mechanical model has been suggested as future work. Before the model can be used to life a CMC, the COD as a function of temperature and stress will have to be known and independently characterized and used as input in the model. Similarly the oxidation kinetics of the matrix is

dependent on the chemistry of the matrix; characterization of the matrix oxidation kinetics is required to use the model reliably.

5.0 Summary

Experimental data on the stress rupture behavior of SiC fiber based tows, minicomposites and ceramic matrix composites (CMCs) in air and moist air are interpreted using a mechanistic model. The kinetics of gaseous diffusion of oxygen and water from the environment through matrix cracks to internal fiber tows, the resulting oxidative loss of BN interphase, the oxidative strength degradation of the SiC fiber tows, and the oxidative sealing of matrix cracks are modeled and integrated within a numerical scheme to predict the stress-rupture behavior of the CMCs or mini-composites. The models for oxidation and/or volatilization of BN and SiC by oxygen and water use available relevant thermodynamic and kinetic data for reactions, vapor pressures, oxygen permeation, and boundary layer effects. Reported data on the kinetics of BN vitalization and SiC oxidation are captured to ensure model verification. The resulting model is compared with experimental data and is shown to capture available data on the stress-rupture data of SiC/BN/SiC CMCs in air and moisture containing atmospheres. An approach to link the model with higher order FEM-based models is suggested.

6.0 Acknowledgments

7.0 References

1. H. E. Eaton and G. D. Linsey, "Accelerated oxidation of SiC CMC's by water vapor and protection via environmental barrier coating approach," *J. Eur. Ceram. Soc.,* 22 2741-2747 (2002).
2. G. Chollon, R. Pailler, R. Naslain, F. Laanani, M. Monthioux, and P. Olry, "Thermal stability of a PCS-derived SiC fibre with a low oxygen content (Hi-Nicalon)," *J. of Mater. Sci.,* 32 327-347 (1997).
3. T. Shimoo, K. Okamura, and F. Toyoda, "Thermal stability of SiO2-coated SiC fiber (Hi-Nicalon) under argon atmosphere," *J. of Mater. Sci.,* 35 3811-3816 (2000).
4. T. Shimoo, T. Morita, and K. Okamura, "Oxidation of Low-Oxygen Silicon Carbide Fibers (Hi-Nicalon) in Carbon Dioxide," *J. Am. Ceram. Soc.`,* 84 [12] 2975-2980 (2001).

5. M. Takeda, J. Sakamoto, Y. Imai, and H. Ichikawas, "Thermal stability of the low-oxygen-content silicon carbide fiber,Hi-Nicalon," *Composite Sci & Tech.,* 59 813-819 (1999).

6. M. Takeda, A. Urano, J. Sakamoto, and Y. Imai`, "Microstructure and oxidative degradation behavior of silicon carbide fiber Hi-Nicalon type S," *J. Nuc. Mater.,* 1998 1594-1599 (1998).

7. R. Q. Yao, Y. Y. Wang, and Z. D. Feng, "The effect of high-temperature annealing on tensile strength and its mechanism of Hi-Nicalon SiC fibres under inert atmosphere," *Fatigue & Fracture of Eng. Mater. & Str.,* 31 777-787 (2008).

8. R. Q. Yao, Z. Feng, L. Chen, Y. Zhang, and B. Zhang, "Oxidation behavior of Hi-Nicalon SiC monofilament fibres in air and O2–H2O–Ar atmospheres," *Corrosion science,* 57 182-191 (2012).

9. R. S. Hay, G. E. Fair, R. Bouffioux, E. Urban, J. Morrow, A. Hart, and M. Wilson, "HiNicalonS SiC fiber oxidation and scale crystallization kinetics," *J. Am. Ceram. Soc.,* 94 [11] 3983-3991 (2011).

10. R. S. Hay, G. E. Fair, R. Bouffioux, E. Urban, J. Morrow, A. Hart, and M. Wilson, "Relationships between fiber strength, passive oxidation and crystallization kinetics of HiNicalonS SiC fibers," *Ceram. Eng. Sci. Proc.,* 32 (2011).

11. D. Gosset, C. Colin, A. Jankowiak, T. Vandenberghe, and N. Lochet, "X-ray Diffraction Study of the Effect of High-Temperature Heat Treatment on the Microstructural Stability of Third-Generation SiC Fibers," *J. Am. Ceram. Soc.,* 96 [5] 1622-1628 (2013).

12. J. J. Sha, T. Nozawa, J. S. Park, Y. Katoh, and A. Kohyama, "Effect of heat treatment on the tensile strength and creep resistance of advanced SiC fibers," *Journal of Nuclear Materials,* 329-333 592-596 (2004).

13. G. N. Morscher, "Tensile Stress Rupture of SiCf/SiCm Minicomposites with Carbon and Boron Nitride Interphases at Elevated Temperatures in Air," *J. Am. Ceram. Soc.,* 80 [8] 2029-2042 (1997).

14. G. N. Morscher, J. Hurst, and D. Brewer, "Intermediate-Temperature Stress Rupture of a Woven Hi-Nicalon, BN-Interphase, SiC-Matrix Composite in Air," *J. Am. Ceram. Soc.,* 83 [6] 1441-1449 (2000).

15. J. J. Brennan, "Interfacial characterization of a slurry-cast melt-infiltrated SiC/SiC Ceramic-Matrix Composite," *Acta Mater.,* 48 4619-4628 (2000).

16. T. A. Parthasarathy, C. P. Przybyla, R. S. Hay, and M. K. Cinibulk, "Modeling the environmental degradation of SiC-based fibers," *J. Am. Ceram. Soc.,* 99 [5] 1725-1734 (2016).

17. N. S. Jacobson, G. N. Morscher, D. R. Bryant, and R. E. Tressler, "High-Temperature Oxidation of Boron Nitride: II, Boron Nitride Layers in Composites," *J. Am. Ceram. Soc.,* 82 [6] 1473-1482 (1999).

18. A. G. Evans, F. W. Zok, R. M. McMeeking, and Z. Z. Du, "Models of High Temperature, Environmentally Assisted Embrittlement in Ceramic-Matrix Composites," *J. Am. Ceram. Soc.,* 79 [9] 2345-2352 (1996).

19. E. J. Opila, J. L. Smialek, R. C. Robinson, D. S. Fox, and N. S. Jacobson, "SiC Recession Caused by SiO2 Scale Volatility unde Combustion Conditions: II, Thermodynamics and Gaseous Diffusion Model," *J. Am. Ceram. Soc.,* 82 [7] 1826-1834 (1999).

20. N. S. Jacobson, "Corrosion of Silicon-Based Ceramics in Combustion Environments," *J. Am. Ceram. Soc.,* 76 [1] 3-28 (1993).

21. N. Jacobson, B. Harder, and D. Myers, "Oxidation Transitions for SiC Part I. Active-to-Passive Transitions," *J. Am. Ceram. Soc.,* 96 [3] 838-844 (2013).

22. K. A. Terrani, B. A. Pint, C. M. Parish, C. M. Silva, L. L. Snead, and Y. Katoh, "Silicon Carbide Oxidation in Steam up to 2 MPa," *J. Amer. Ceram. Soc.,* 97 [8] 2331-2352 (2014).

23. E. J. Opila, D. S. Fox, and N. S. Jacobson, "Mass Spectrometric Identification of Si-O-H (g) Species from the Reaction of Silica with Water Vapor at Atmospheric Pressure," *J. Am. Ceram. Soc.,* 80 [4] 1009-1012 (1997).

24. E. J. Opila, "Variation of the Oxidation Rate of Silicon Carbide with Water Vapor Pressure," *J. Am. Ceram. Soc.,* 82 [3] 625-636 (1999).
25. J. Jung, B. C. Do, and Q. D. Yang, "Augmented finite-element method for arbitrary cracking and crack interaction in solids under thermo-mechanical loadings," *Phil. Mag. A,* A374 (2016).
26. N. Naderi, J. Jung, and Q. D. Yang, "A three dimensional augmented finite element for modeling arbitrary cracking in solids," *Int. J. of Frac.,* 197 147-168 (2016).
27. I. Barin, "Thermochemical Data of Pure Substances I, ," *VCH Verlagsgesellschaft: New York* (1995).
28. N. S. Jacobson, E. J. Opila, D. L. Myers, and E. H. Copland, "Thermodynamics of gas phase species in the Si–O–H system," *J. Am. Ceram. Soc.,* 37 1130-1137 (2005).
29. A. Plyasunov, "Thermodynamic properties of H4SiO4 in the ideal gas state as evaluted from experimental data," *Geochemica et Cosmochimica Acta,* 75 3853-3865 (2011).
30. R. A. Svehla, "Estimated viscosities and thermal conductivities of gases at high temperatures," *NASA Tech report R-132* (1962).
31. T. Parthasarathy, R. Rapp, M. Opeka, and M. Cinibulk, "Modeling Oxidation Kinetics of SiC-Containing Refractory Diborides," *Journal of the American Ceramic Society,* 95 [1] 338-349 (2012).
32. T. Shimoo, F. Toyoda, and K. Okamura, "Oxidation kinetics of low-oxygen silicon carbide fiber," *J Mater. Sci.,* 35 3301-3306 (2000).
33. G. N. Morscher, "Tensile Stress Rupture of SiC/SiC Minicomposites with Carbon and Boron Nitride Interphases at Elevated Temperatures in Air," *J. Am. Ceram. Soc.,* 80 [8] 2029-2042 (1997).
H. M. Yun and J. A. DiCarlo, "Time/Temperature Dependent Tensile Strength of SiC and A1203-Based Fibers." In. NASA, 1996.
35. W. Gauthier and J. Lamon, "Delayed Failure of Hi-Nicalon and Hi-Nicalon S Multifilament Tows and Single Filaments at Intermediate Temperatures (5001–8001C)," *J. Am. Ceram. Soc.,* 92 [3] 702-709 (2009).
36. D. Marshall and O. Sudre, "Stress rupture behavior of S200H CMCs," *unpublished work, Teledyne Scientific, Thousand Oaks, CA* (2016).
37. L. P. Zawada and J. Pierce, "Stress Rupture of S200H CMC," *unpublished work, Air Force Reserach Lab., WPAFB, OH* (2016).
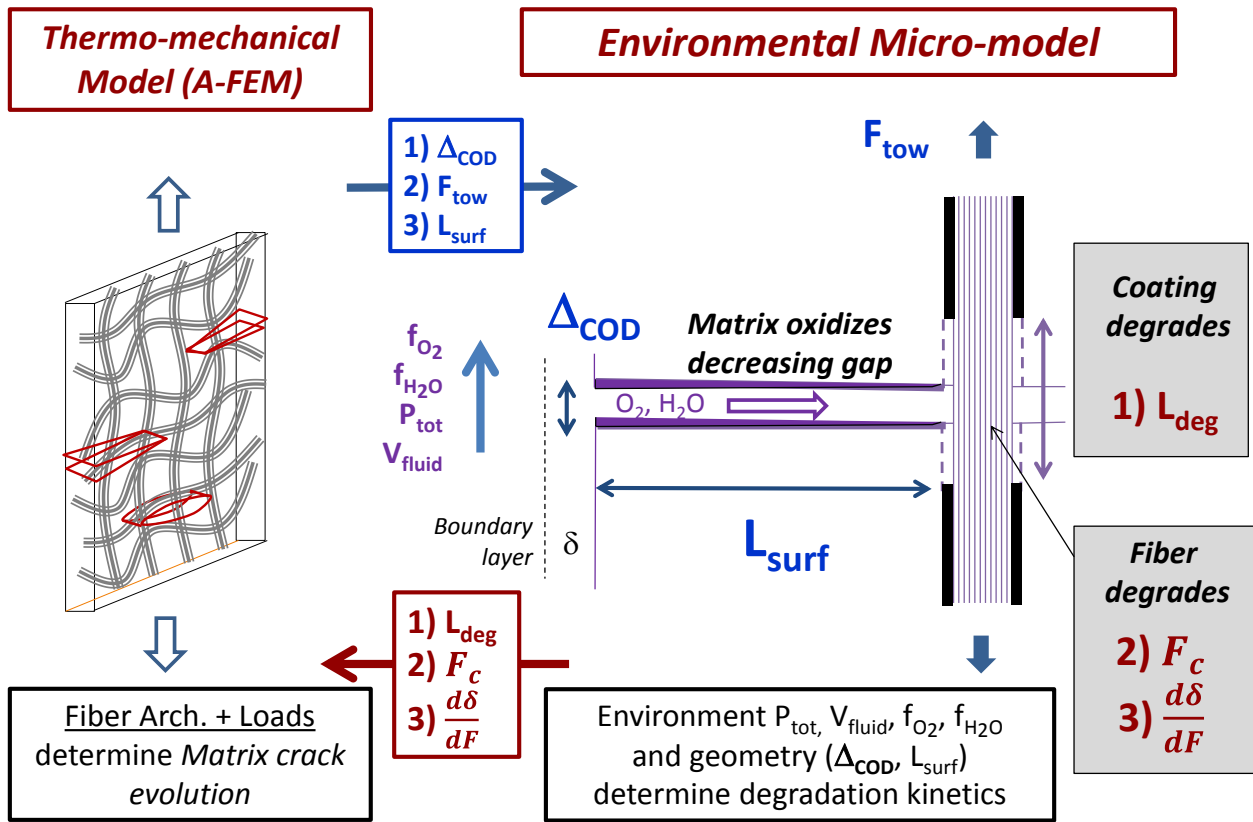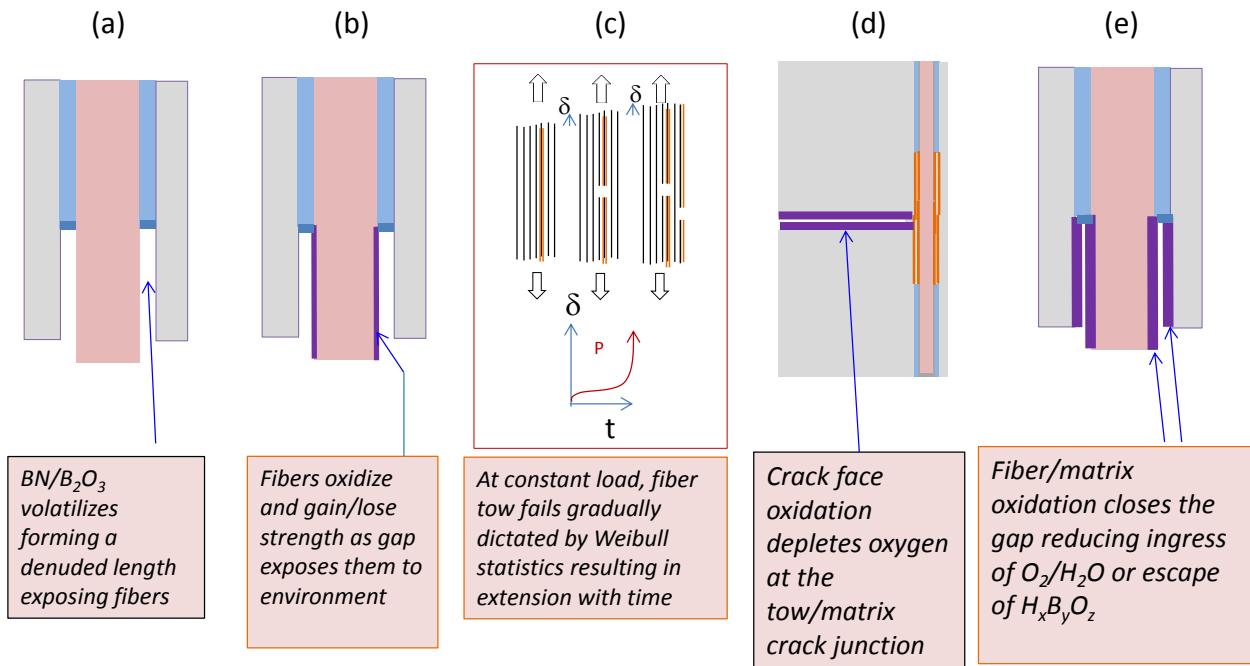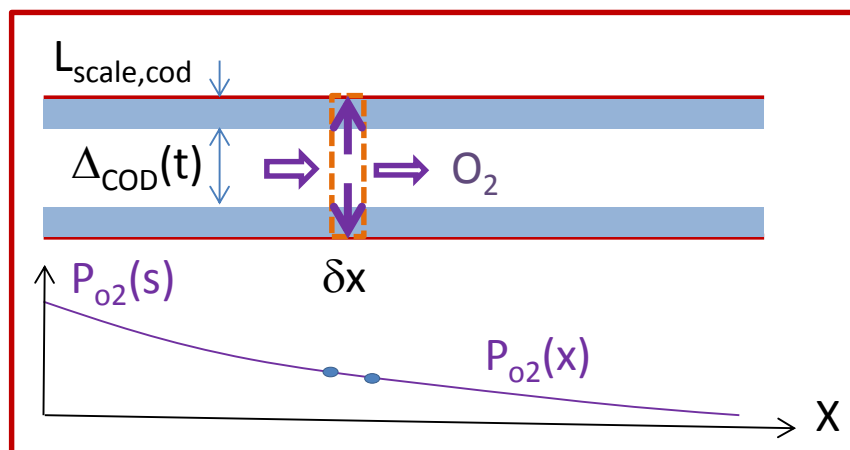
Figure 1: An overview of the spatio-temporal environmental degradation model

Figure 2: Key mechanisms that dominate the environmental degradation of CMCs under turbine engine conditions

Figure 3: Modeling the gradient in partial pressure of oxygen from the surface along the matrix crack opening. Within an infinitesimal width, the incoming and outgoing oxygen flux as well as that used for scale formation are balanced.
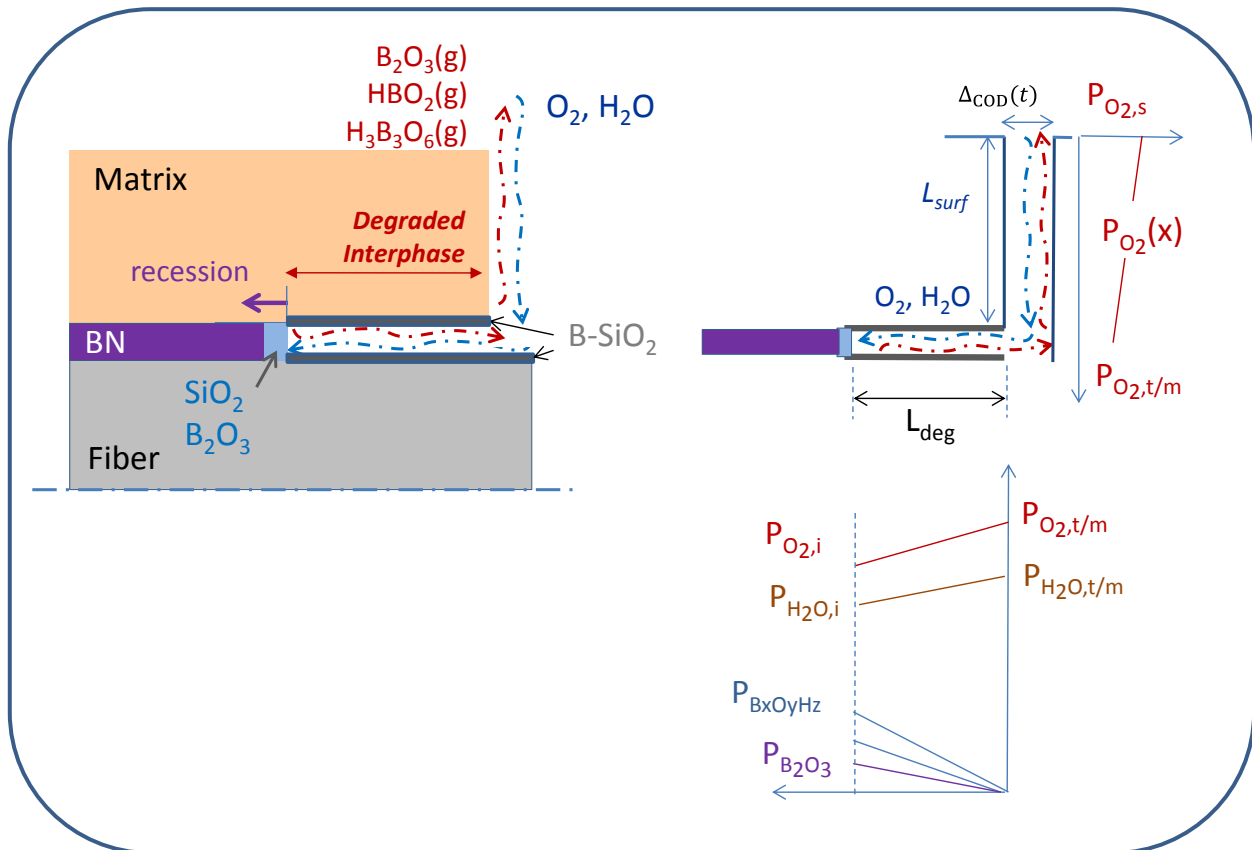
Figure 4 : Modeling the interfacial degradation kinetics. The partial pressures of the reactant and product gases determine the kinetics of flux of the gases and thus the kinetics of the degradation length.
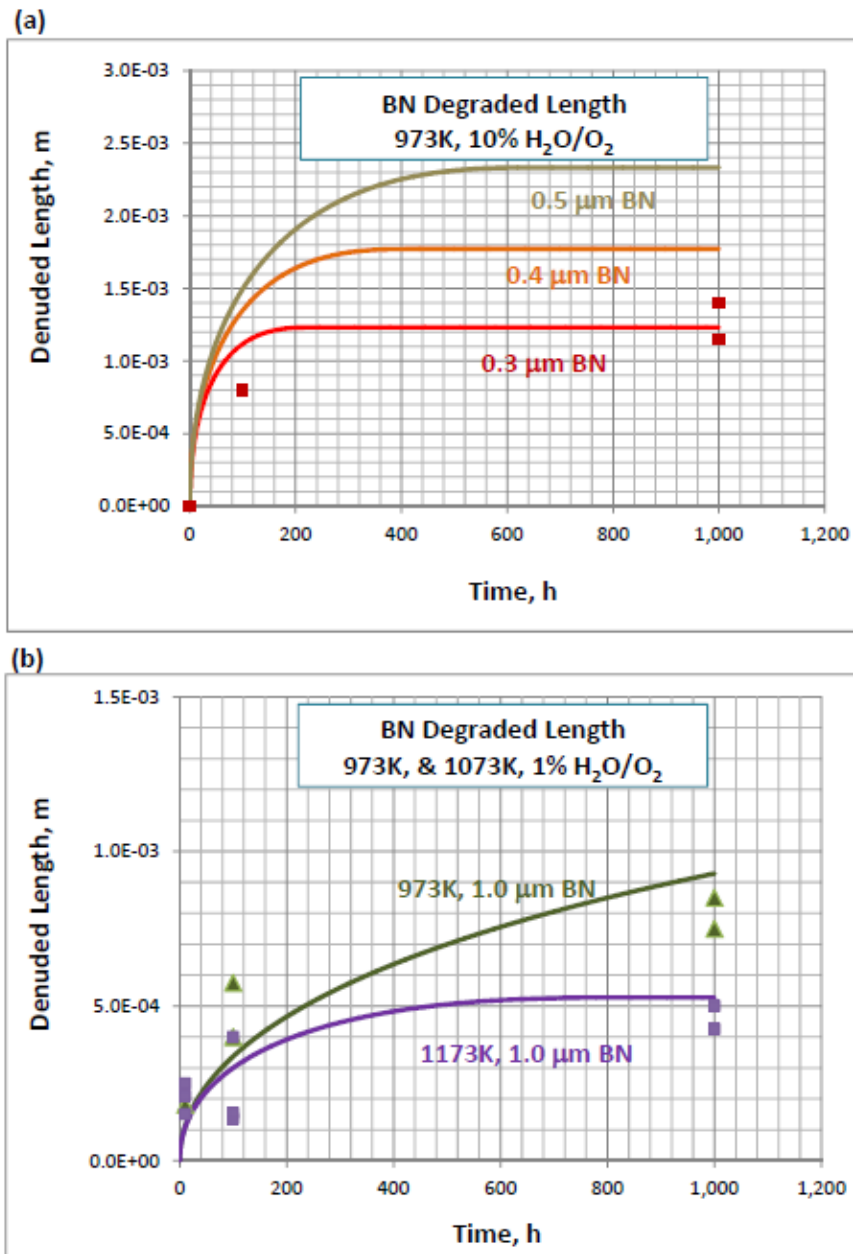
Figure 5: The model predictions for the degraded interphase length as a function of time at different temperatures and environment are shown In comparison to the experimental data of Jacobson et al.
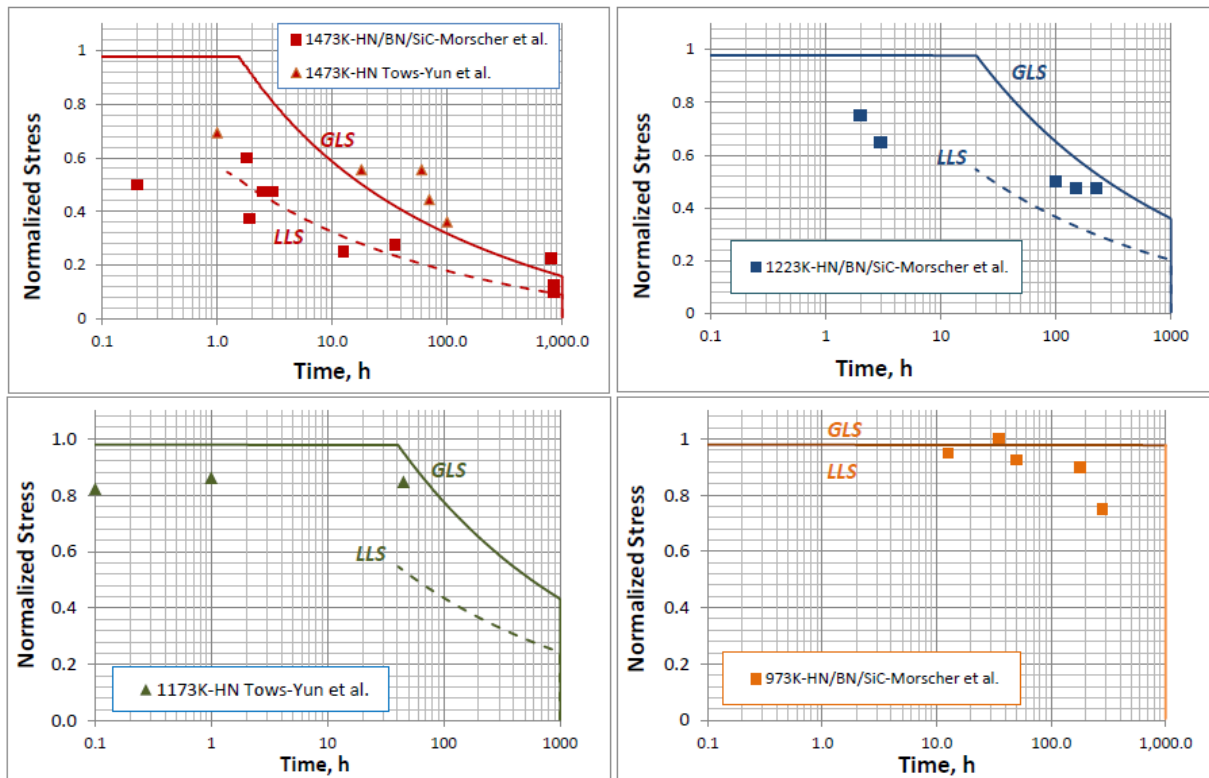
Figure 6: A comparison of the model predictions for stress-rupture in air for the two bounds, GLS and LLS, shown here in comparison to data on tows by Yun et al., and miniCMCs by Morscher et al.
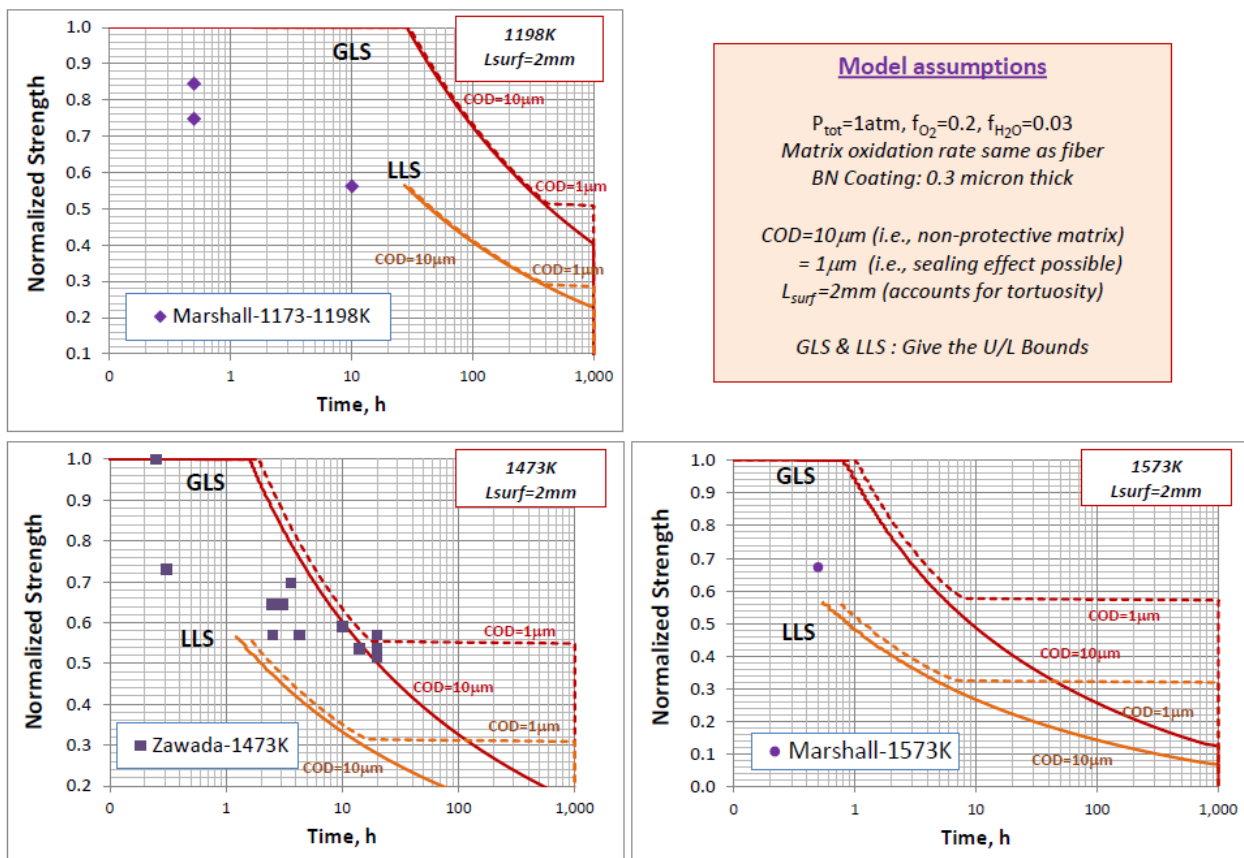
Figure 7 Model predictions for the stress rupture of S200H CMCs, shown for the bounds GLS and LLS, for different values of crack opening displacements of 10 and 1 microns. The experimental data of Zawada et al., and Marshall et al. are shown for comparison
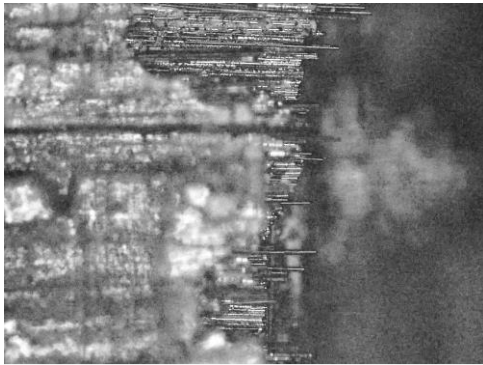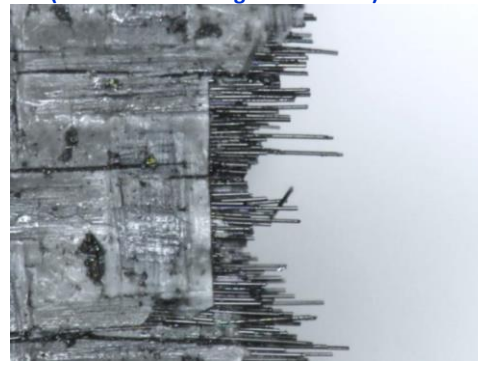
Figure 8: Fracture surfaces of two samples of S200H tested under the same conditions showing different fracture morphologies, that correspond to brittle flat fracture for the shorter life sample, and fibrous fracture for the longer life sample, supporting the model in using GLS and LLS to predict upper and lower bounds for life.
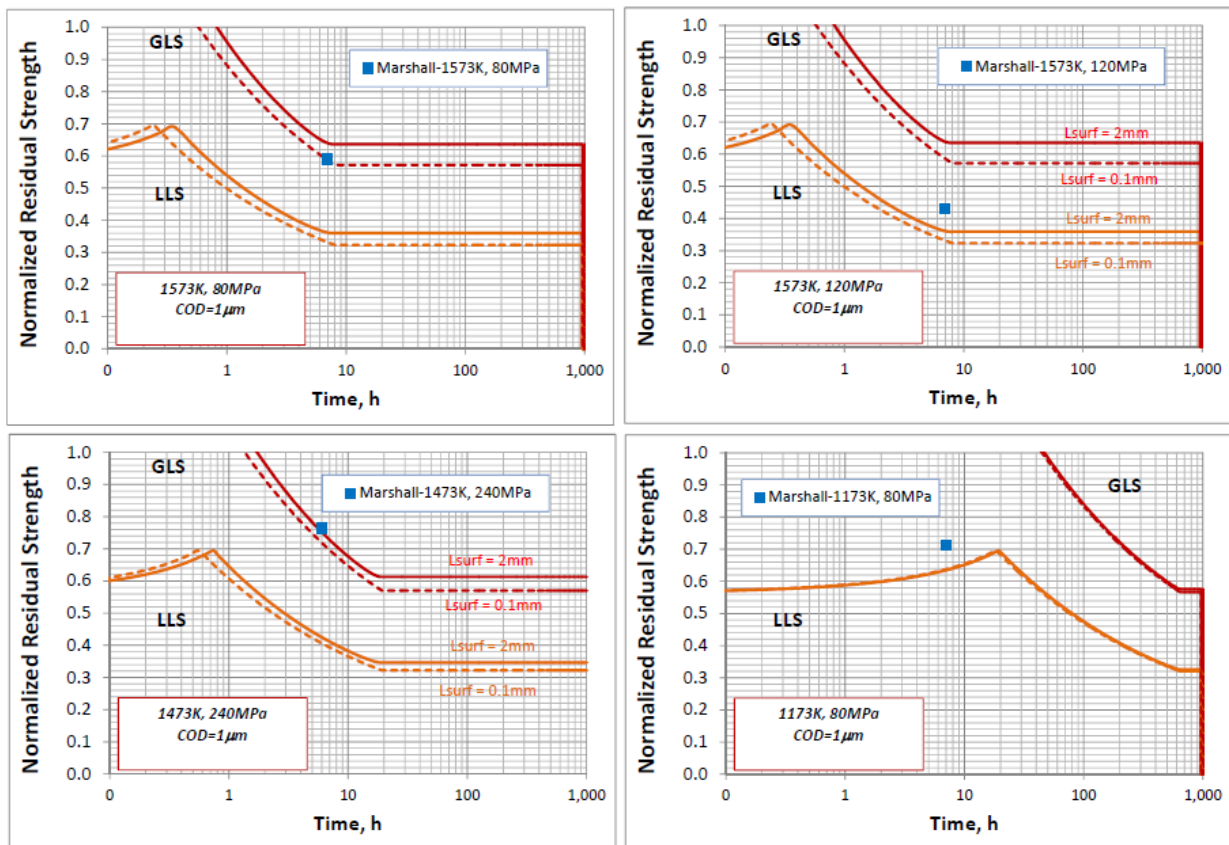

Figure 9: Model predictions for residual strength of S200H CMCs after exposure under stress and tested at R.T., compared with data obtained after exposure to ambient air under different conditions (a) 1573K. 80 MPa (b) 1573K, 120 Mpa (c)1473K, 240 Mpa (d) 1173K, 80MPa
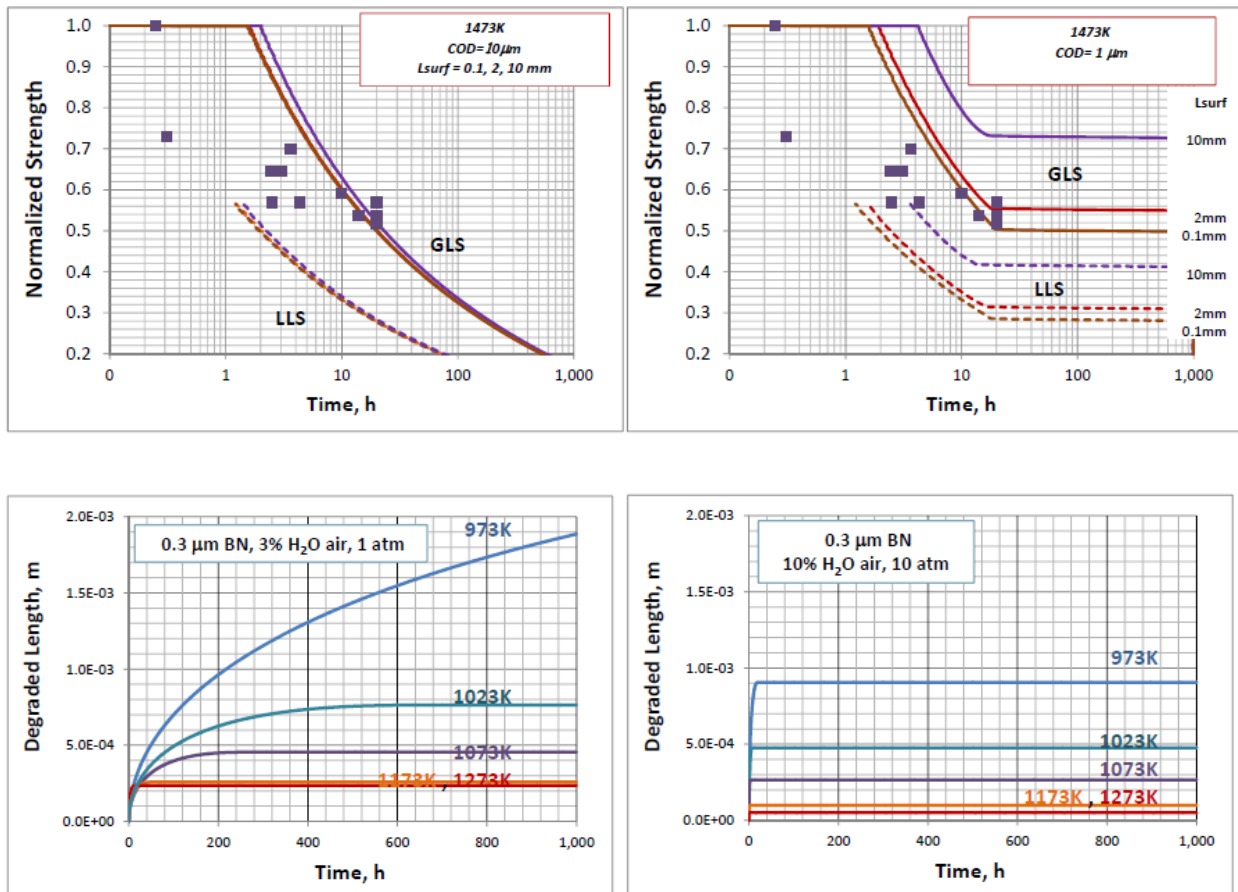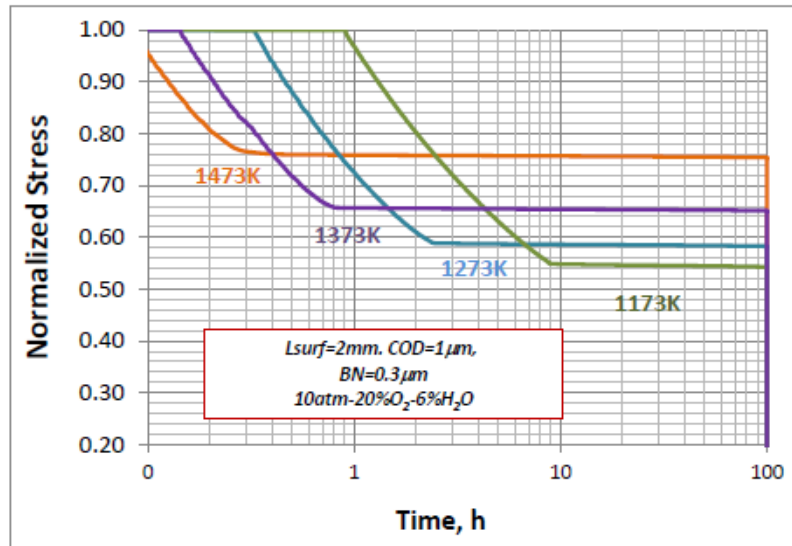
Figure 10: Parametric studies of the model showing the effect of distance of fiber two from surface for (a) large crack opening displacement and (b) small crack opening displacement. The degradation length of the interface for (a) ambient and (b) turbine engine conditions.

Figure 11: Parametric studies of the model showing the effect of temperature on the stress-rupture of a SiC/BN/SiC CMC in an environment representative of the turbine engine conditions. The degradation is faster at higher temperatures, but the time for matrix crack sealing is longer at lower temperature resulting in higher degradation with time.